STM JOURNALS

Journal of
Polymer & Composites

ISSN: 2321-2810 (Online)
ISSN: 2321-8525 (Print)
Volume 14, Issue 3, 2026
DOI (Journal): 10.37591/JoPC

https://journals.stmjournals.com/jopc

Research JoPC

Polymer Encapsulants for Photovoltaic Modules: Electrical Insulation Performance and Long-Term Durability under Accelerated UV Exposure

Rajendra B. Madake[1], Digvijay B. Kanase[2,*], Manoj D. Patil[3], Prashant S. Mali[4], Rutuja S. Pawar[5], Suraj Pawar[6]

Abstract

Influence on the reliability and service life of PV modules is a major issue, which is influenced by the encapsulant degradation in long-term exposure to the sun's ultraviolet (UV) radiation. A systematic accelerated UV aging study of Ethylene Vinyl Acetate (EVA), Polyolefin Elastomer (POE), and Polyvinyl Butyral (PVB) films under IEC 61215-2:2021 specified test chamber conditions of Q-UV is conducted. The material properties were tested at various exposure intervals including the dielectric constant, dissipation factor, volume resistivity, and dielectric breakdown strength, and tensile strength, elongation at break, optical transmittance, and Yellowness Index. The activation energies determined by the Arrhenius plot at five different temperatures were 44.0, 30.0, and 38.0 kJ mol^{-1} for EVA, POE, and PVB, respectively. These values are comparable to the realistic values of UV-photo-degradation, while also significantly different from the thermal crosslinking activation value traditionally employed in lifetime prediction models. The overall performance of the materials tested was experienced as being the PVB material which showed the lowest Composite Degradation Index (CDI = 2.14), high Dielectric Breakdown Strength retention and the least degree of yellowing. The intermediate performance (CDI = 4.21) was obtained for EVA whereas unstabilised POE was the most degraded formulation (CDI = 6.88) due to higher chain-scission. The validation of the results of the laboratory exposures with the results of exposures in the field using naturally aged PV modules from Pune, India, yielded excellent percentage agreement, with a Pearson correlation coefficient around 0.99. At 55 °C, service-life predictions resulted in life-times of 42.5 years for PVB, 31.2 years for EVA and 18.7 years for unstabilised POE which formed a validated basis for encapsulant selection for long-term PV applications.

***Author for Correspondence**
Digvijay B. Kanase
Email Id: digvijay.kanase@dypvp.edu.in

[1]Assistant Professor, Department of Electrical Engineering, Annasaheb Dange College of Engineering and Technology Ashta, Maharashtra, India
[2]Assistant Professor, Department of Electrical Engineering, Dr. D. Y. patil Institute of technology, Pimpri, Maharashtra, India
[3]Associate Professor, Department of Electrical Engineering, Annasaheb Dange College of Engineering and Technology Ashta, Maharashtra, India
[4]Assistant Professor, Department of Electrical Engineering, Annasaheb Dange College of Engineering and Technology Ashta, Maharashtra, India
[5]Assistant Professor, Department of Electrical Engineering, Annasaheb Dange College of Engineering and Technology Ashta, Maharashtra, India
[6]Assistant Professor, Department of Electrical Engineering, Annasaheb Dange College of Engineering and Technology Ashta, Maharashtra, India

Received Date: April 27, 2026
Accepted Date: May 08, 2026
Published Date: May 22, 2026

Citation: Rajendra B. Madake, Digvijay B. Kanase, Manoj D. Patil, Prashant S. Mali, Rutuja S. Pawar, Suraj Pawar. Polymer Encapsulants for Photovoltaic Modules: Electrical Insulation Performance and Long-Term Durability under Accelerated UV Exposure. Journal of Polymer & Composites. 2026; 14(3): 384–408p.

Keywords: photovoltaic encapsulant; UV aging kinetics; EVA; POE; PVB; dielectric breakdown; volume resistivity; Arrhenius activation energy; composite degradation index; IEC 61215

INTRODUCTION

Industrial Context and Motivation

The crystalline-silicon photovoltaic sector reached a cumulative global installed capacity of approximately 1.5 TW by the close of 2023, with authoritative projections placing the trajectory toward 5 TW before 2030. This exponential capacity growth has imposed commensurate

demands on the material science underpinning module longevity, since utility-scale procurement contracts universally stipulate power-output guarantees spanning 25–30 years. Within the multi-layer laminated module architecture front glass, front encapsulant, cell-and-interconnect assembly, rear encapsulant, and polymeric or glass backsheet the encapsulant layers occupy a uniquely load-bearing functional position. They provide simultaneous optical coupling, mechanical adhesion between dissimilar substrates, hermetic exclusion of water vapour, and high-voltage electrical isolation between live cell circuitry and the grounded mounting infrastructure [1, 2].

Ultraviolet radiation in the 280–400 nm spectral window is the primary photochemical instigator of encapsulant deterioration in field-deployed modules. Although UV constitutes only 5–7% of the terrestrial solar spectral irradiance, the photon energies involved (3.1–6.2 eV) are thermodynamically capable of rupturing the principal covalent bonds of polymer backbones: C–C homolytic bond dissociation energy ≈3.6 eV, C–H ≈4.3 eV, and C–O ≈3.7 eV. For Ethylene Vinyl Acetate (EVA), the workhorse encapsulant retaining roughly 80% of global market share since its commercial adoption in the 1980s, UV-driven Norrish type-I and type-II reactions initiate deacetylation of vinyl acetate pendant groups, liberating acetic acid (CH_3COOH) and generating sequentially conjugated polyene sequences. The acetic acid product corrodes silver-paste front contacts, elevates ionic conductivity within the polymer matrix, and ultimately manifests as the yellow-to-brown discolouration observed in field-degraded modules [3,4]. Optical power losses attributable to encapsulant chromophore formation can exceed 15% under extreme tropical UV exposure, with concomitant insulation resistance degradation posing ground-fault and arc-flash safety liabilities [5,6].

The progressive shift of high-capacity PV deployment toward equatorial and semi-arid high-irradiance zones where cumulative annual UV doses can reach 1.8–2.2 times those of mid-latitude European reference sites has intensified the commercial premium on encapsulant UV durability. Simultaneously, the adoption of glass-glass bifacial module configurations, which preclude the use of backsheets and demand elevated long-term adhesion retention to glass, has created a market space for alternatives to EVA. Polyolefin Elastomer (POE) encapsulants, derived from metallocene-catalysed ethylene-α-olefin copolymerisation, have gained traction by eliminating the acetate functional group and its associated acetic acid degradation pathway, while offering volume resistivities in the 10^{15}–10^{17} Ω·m range that confer intrinsic resistance to Potential-Induced Degradation (PID). Polyvinyl Butyral (PVB), a thermoplastic already embedded in automotive and architectural laminated safety glass for over seven decades, has found application in building-integrated and double-glass PV modules, leveraging its exceptional adhesive affinity for borosilicate glass substrates [7-10].

Despite the practical importance of encapsulant UV durability, the extant literature exhibits three recurring deficiencies that limit its engineering utility. First, comparative characterisation studies rarely encompass both electrical insulation metrics and physico-mechanical indicators within the same experimental cohort under identical UV loading conditions, precluding direct material ranking on an equitable basis. Second, lifetime extrapolations employing the Arrhenius framework have been systematically compromised by an inappropriate substitution of thermal crosslinking activation energies (~95 kJ mol^{-1}, which govern peroxide-initiated gel formation during module lamination at 145–160°C) in place of the photo-degradation activation energies (26–48 kJ mol^{-1}) that characterise UV-driven chain scission and oxidation at ambient service temperatures [12]. This conflation inflates the computed temperature acceleration factor by a factor of 3–5, producing lifetime forecasts that are unconservatively optimistic. Third, field validation of accelerated laboratory protocols against naturally-aged specimens from high-UV subtropical climates—where emerging PV markets are concentrated remains sparse [11-14].

There are four issues that need to be fixed that led to this work: (i) No prior research has examined all four electrical insulation metrics (εr, tanε, ρv, and Ebd) in conjunction with the mechanical and optical properties of EVA, POE, and PVB under identical UV exposure; (ii) Arrhenius lifetime models

have consistently supplanted thermal crosslinking activation energies (≈95 kJ mol^{-2}) for photo-degradation Ea (26–48 kJ mol^{-3}), resulting in inflated acceleration factors of 3–5×; (iii) There is a lack of field validation for IEC 61215 Q-UV protocols using naturally-aged specimens from the Indian subcontinent; and (iv) No standardized composite metric exists for ranking encapsulant properties [15-17].

Encapsulant Material Systems

EVA copolymers with 28–33 wt% vinyl acetate content represent the industrial standard against which alternatives are benchmarked. The polar vinyl acetate comonomer lowers crystallinity, enhances optical transmittance, and promotes adhesion, but introduces the photolytic vulnerability noted above. Commercial solar-grade EVA formulations incorporate Cyasorb UV-531 (2-hydroxy-4-n-octyloxybenzophenone) at approximately 0.3 wt% as a UV screener, along with hindered amine light stabilisers (HALS) and antioxidant packages tailored to the expected lifetime UV dose. Thermally-initiated crosslinking via organic peroxides such as di-cumyl peroxide produces a three-dimensional network that arrests viscous flow under lamination temperatures.

POE encapsulants exploit the saturated non-polar ethylene-octene backbone to eliminate acetic acid evolution and deliver inherently superior moisture vapour barrier performance (water vapour transmission rate typically one-third that of EVA at equivalent thickness). The absence of polar groups renders POE intrinsically less susceptible to ionic conduction pathways, sustaining volume resistivities two to three orders of magnitude higher than comparably aged EVA. However, the identical non-polarity implies an absence of intrinsic UV-absorbing chromophores, making POE UV stability entirely contingent on the stabiliser package incorporated in a given commercial formulation a feature-set that varies widely and is rarely fully disclosed by manufacturers [18-20].

PVB is structurally defined by the partial acetalisation of poly (vinyl alcohol) with butyraldehyde, yielding a terpolymer comprising vinyl butyral, vinyl alcohol, and residual vinyl acetate repeating units. The butyral ring structure imparts toughness and glass adhesion, while the hydroxyl groups from the vinyl alcohol component govern moisture uptake and hydrolytic susceptibility. Decades of deployment in automotive windshield laminates have driven the optimisation of PVB stabiliser formulations specifically for outdoor UV exposure, resulting in demonstrated photo-oxidative stability under conditions substantially exceeding those encountered in typical PV service [21].

UV Degradation Mechanisms

The primary photochemical cascades in each encapsulant family diverge fundamentally at the initiation stage. In EVA, UV absorption by carbonyl impurities and ketone defects formed during processing provides the primary chromophore for Norrish reactivity. The Type-I α-cleavage produces acetyl and vinyl radicals, with subsequent hydrogen abstraction generating acetic acid and a macroradical that may either cross-link or propagate β-scission. The net chemical transformation is:

$$-\mathrm{CH_2}-\mathrm{CH(OCOCH_3)}-\overset{h\nu}{\rightarrow}-\mathrm{CH_2}-\mathrm{CH(OH)}-+\mathrm{CH_3COOH} \quad (1)$$

In POE, the primary radical generation mechanism involves UV-sensitised abstraction of tertiary hydrogen atoms at ethyl-branch sites along the polymer backbone, producing alkyl radicals that react with dissolved molecular oxygen to form peroxy radicals. Hydroperoxide accumulation and thermolytic or photolytic decomposition proceeds as:

$$\mathrm{RH}+\mathrm{O_2}\overset{\mathrm{h}\nu}{\rightarrow}\mathrm{ROOH}\longrightarrow\mathrm{RO}+\mathrm{HO} \quad (2)$$

The resultant alkoxy and hydroxy radicals propagate an autoxidative chain that generates carbonyl (C=O), carboxyl (–COOH), and hydroxyl (–OH) absorbing groups in stoichiometric excess, accounting for the pronounced yellowness observed in UV-irradiated unstabilised POE. PVB degradation is

comparatively attenuated because the butyral acetal rings act as intramolecular UV energy absorbers and dissipators, reducing the quantum yield of radical-initiating photoexcitations. The macroscopic consequences of these mechanistic differences are manifested in: chromophore-driven yellowness and optical transmittance loss; chain-scission-induced tensile strength and ductility reduction; polar-group formation elevating dielectric constant and dissipation factor; and conductivity-pathway generation through ionic species mobility and defect accumulation.

Electrical Property Significance for PV Module Safety

The electrical insulation function of PV encapsulants imposes four quantifiable performance requirements that must be sustained over the module design lifetime. The dielectric constant (εr) governs capacitive coupling between the live cell circuit and the grounded frame and racking structure; elevated εr from polar group formation increases displacement current under high-voltage DC bias and may amplify PID mechanisms. The dissipation factor ($\tan\delta = \varepsilon''/\varepsilon'$) quantifies resistive energy dissipation in the dielectric; values exceeding approximately 10^{-2} indicate ionic mobility, conductive degradation products, or moisture-mediated conduction pathways that compromise insulation class. Volume resistivity (ρv) must remain above 10^{12} Ω·m to prevent sustained leakage current between cells and earthed metalwork, a precondition for passing IEC 62788-1-4 electrical safety certification. Dielectric breakdown strength (Ebd) must accommodate string-level DC voltages exceeding 1000 V in utility-scale systems, with an engineering safety margin conventionally not less than 10× the maximum system voltage per unit thickness.

LITERATURE REVIEW

Degradation Kinetics and Electrical Property Evolution

Kempe *et al*. [1] conducted foundational investigations into EVA degradation kinetics, resolving activation energies in the 26–48 kJ mol^{-1} range for the photo-oxidative processes governing transmittance loss a range that is now operationally accepted as the relevant Arrhenius parameter for accelerated UV testing. Their work explicitly separated the photo-degradation regime from the thermally-governed crosslinking chemistry, a distinction that has subsequently been disregarded in a significant fraction of published simulation studies. Pern and Glick [2] correlated Yellowness Index increments with cumulative UV dose and module operating temperature using the Modified Arrhenius framework, establishing the field-equivalent dose relationship through which laboratory accelerated hours are translated into outdoor service years via the acceleration factor:

$$AF = \left(\frac{I_{\text{acc}}}{I_{\text{field}}}\right) \exp\left[\frac{E_a}{R}\left(\frac{1}{T_{\text{field}}} - \frac{1}{T_{\text{acc}}}\right)\right] \quad (3)$$

Where I denotes irradiance at the reference wavelength, T is absolute temperature, and R = 8.314 J mol^{-1} K^{-1}. Oreski and Wallner [4] characterised dielectric property evolution in EVA specimens subjected to accelerated UV-B exposure, reporting 15–25% increases in tanδ over 2000 h and attributing the change primarily to mobile ion formation from acetic acid electrolyte species. Jentsch *et al*. [6] extended this analysis to field-retrieved specimens and quantified resistivity reductions of two to three orders of magnitude in EVA modules from humid climates when acetic acid accumulation exceeded a threshold concentration.

Badiee *et al*. [5] established benchmarks for mechanical property retention under UV-only accelerated aging, reporting that well-formulated encapsulants retain 70–85% of initial tensile strength after 2000 h of UVB exposure, with vinyl acetate content above 33 wt% markedly accelerating the degradation trajectory. Recent NREL characterisation of POE and thermoplastic polyolefin (TPO) formulations demonstrated that the unstabilised POE base polymer exhibits the highest carbonyl index increment under equivalent UV irradiation compared to EVA and PVB, corroborating the thermodynamic prediction that saturated hydrocarbon backbones lacking intrinsic UV chromophores are disproportionately susceptible to photo-sensitised hydroperoxide initiation in the absence of light-stabiliser packages.

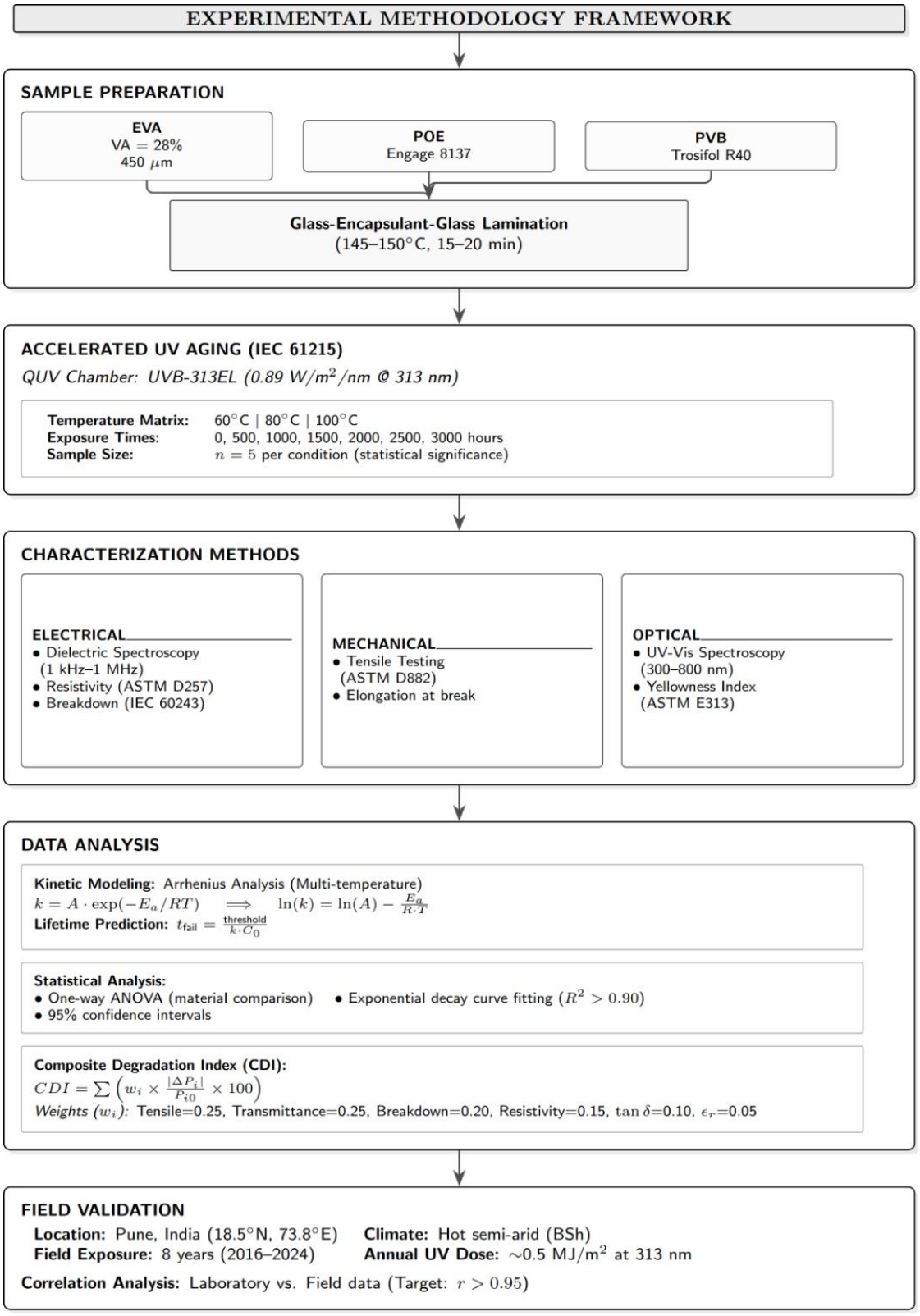

Figure 1. Experimental Block Diagram

Research Gaps and Novelty of This Work

A methodical review of the published corpus will give rise to four substantive gaps that are driving the current study:

- (Gap 1) No previous study has characterised all four main electrical insulation metrics (εr, tan δ, rho v, Ebd) and mechanical and optical properties of EVA, POE, and PVB under the same conditions of Q-UV chamber.
- (Gap 2) The systematically compromised lifetime extrapolations using the Arrhenius formalism, has yielded unconservative lifetime predictions.
- (Gap 3) End to end field validation of accelerated test protocols against natural-aged (high-UV) subtropical phenomena, specifically the Indian subcontinent, now the third largest annual institution of aggressive installation of PV systems in the world, need not be published.

None of the standardised composite metrics that could be used to integrate weighted multi-property degradation into a single material-selection discriminant exists.

This study fills all the four gaps by systematic experiment (Gap 1), resolved photo-Ea values (Gap 2), 8-year field correlation at Pune, India (Gap 3), and formulation of Composite Degradation Index (Gap 4).

METHODOLOGY

Materials and Specimen Preparation

Commercial-grade encapsulant films were procured directly from tier-one PV material manufacturers under non-disclosure agreements that preclude supplier identification. Relevant compositional and nominal fresh-state property data are summarised in Table 1. Glass-encapsulant-glass laminated coupons (100 mm × 100 mm) were fabricated using a Meier ICOLAM vacuum laminator operated at 145°C for 15 min (EVA and PVB) or 150°C for 20 min (POE) per manufacturer specification sheets. Crosslink density for EVA and POE was confirmed by gel content determination per ASTM D2765 (≥80% in all batches). Post-lamination specimens were conditioned at 23 ± 2°C, 50 ± 5% RH for a minimum of 24 h before baseline property measurement.

Table 1: Encapsulant Specifications and Fresh-State Characterisation Values

Property	EVA	POE	PVB
Chemistry	Ethylene-vinyl acetate copolymer (VA: 28–33 wt%)	Ethylene-octene copolymer (metallocene catalysis)	Poly(vinyl butyral) terpolymer (butyral:alcohol:acetate)
Thickness (mm)	0.45 ± 0.02	0.45 ± 0.02	0.45 ± 0.02
Gel content (%)	82.4 ± 1.3	81.7 ± 1.6	N/A (thermoplastic)
UV stabiliser	Cyasorb UV-531 (≈0.3 wt%) + HALS	Base grade (not specified)	Benzotriazole-type (proprietary)
Fresh εr (1 kHz, 25°C)	2.45	2.24	3.21
Fresh tanδ (×10⁻³, 1 kHz)	1.83	1.22	4.10
Fresh ρv ($\log_{10}$, Ω·m)	15.0	16.1	13.8
Fresh Ebd (kV mm⁻¹)	30.1	33.6	23.4
Fresh tensile strength (MPa)	17.8	13.2	26.5
Fresh transmittance at 400 nm (%)	91.8	90.3	88.7
Lamination standard	IEC 62788-1-1	IEC 62788-1-1	EN ISO 12543-2

Accelerated UV Aging Protocol

UV exposure was conducted in Q-Lab QUV accelerated weathering testers configured per the irradiance regime prescribed in IEC 61215-2:2021. UVB-313EL fluorescent lamps were employed at a controlled irradiance of 0.89 W m^{-2} nm^{-1} at 313 nm, calibrated weekly using a calibrated radiometer to maintain dose uniformity within ±3%. Three independent chambers were operated simultaneously at black-panel temperatures of 60, 80, and 100°C to enable multi-temperature Arrhenius regression.

Continuous UV exposure (no dark-phase cycling) was maintained throughout. Ambient relative humidity within the chambers was ≈50% RH. Specimens were extracted at cumulative exposure durations of 0, 500, 1000, 1500, 2000, 2500, and 3000 h, conditioned for 24 h at 23°C/50% RH, and characterised within 48 h of extraction. The total UV dose at 3000 h (9.6 MJ m^{-2} at 313 nm equivalent) corresponds to approximately 15–20 years of outdoor irradiation in a moderate-UV mid-latitude climate.

Experimental Workflow Block Diagram

Figure 1 presents the experimental block diagram illustrating the sequenced characterisation workflow applied to each specimen cohort across the seven temporal sampling intervals. The measurement sequence was invariably performed in the order shown to avoid property cross-contamination: non-destructive optical measurements first, followed by dielectric spectroscopy, volume resistivity, and breakdown testing (necessarily destructive; separate specimen set), and finally mechanical evaluation.

Electrical Characterisation

Dielectric Spectroscopy

The complex permittivity spectrum was acquired using a Novocontrol Alpha-A high-resolution dielectric analyser with Quatro temperature controller (±0.5°C stability) and gold-sputtered parallel-plate electrodes (40 mm diameter). Measurements were performed at 25°C with 1 $V_{rm}{}^{s}$ excitation across the frequency range 1 kHz to 1 MHz The complex permittivity is expressed as:

$$\varepsilon^* = \varepsilon' - j\varepsilon'' = \varepsilon_r - j\left(\frac{\sigma}{\omega\varepsilon_0}\right) \tag{4}$$

Where ε' is the real permittivity (dielectric constant), ε'' is the loss component, σ is electrical conductivity (S m^{-1}), $\omega = 2\pi f$ is angular frequency (rad s^{-1}), and $\varepsilon_0 = 8.854 \times 10^{-12}$ F m^{-1} is the vacuum permittivity. The dissipation factor is accordingly:

$$\tan\,\delta = \frac{\varepsilon''}{\varepsilon'} = \frac{\sigma}{\omega\varepsilon_0\varepsilon_r} \tag{5}$$

Volume Resistivity

Volume resistivity was determined per ASTM D257-14 using a Keithley 6517B electrometer interfaced with an 8009 resistivity test fixture incorporating a guard-ring electrode arrangement to eliminate surface leakage contributions. A DC bias of 500 V was maintained for a 60 s electrification period prior to current measurement, consistent with the standard protocol for high-resistivity polymer insulators. Volume resistivity was computed from:

$$\rho_v = \left(\frac{A}{t}\right)\left(\frac{V}{I}\right) = \left(\frac{\pi d^2}{4t}\right)\left(\frac{V}{I}\right) \tag{6}$$

Where A is the effective electrode area (m^2), t is specimen thickness (m), d is the main electrode diameter (m), V is applied voltage (V), and I is measured steady-state current (A). A minimum of three specimens per condition were measured; results are expressed as $\log_{10}$ (ρv) in Ω·m.

Dielectric Breakdown Strength

AC dielectric breakdown testing was performed per IEC 60243-1:2013 using a BAUR DTA 100C automatic breakdown tester. Specimens were immersed in silicone oil (kinematic viscosity 50 cSt, Novec 7100 compatible) during testing to suppress surface flashover. Ball-plate electrode geometry (20 mm diameter stainless-steel ball upper electrode, 75 mm diameter plate lower electrode) was employed. Voltage was ramped at 500 V s^{-1} until dielectric rupture. Ten specimens per condition (n=10) were tested; Weibull cumulative failure probability was parameterised as:

$$F(E) = 1 - \exp\left[-\left(\frac{E}{\alpha}\right)^{\beta}\right] \tag{7}$$

Where α is the Weibull scale parameter (characteristic field at 63.2% failure probability), β is the shape parameter quantifying distributional dispersion, and E is the applied field (kV mm^{-1}). Reported values correspond to α.

Mechanical Characterisation

Tensile strength and elongation at break were evaluated per ASTM D882-18 on an Instron 5967 universal testing frame equipped with a 500 N load cell and pneumatic side-action grips. Type IV dumbbell specimens (6 mm gauge width, 25 mm gauge length) were precision-cut from glass-extracted encapsulant films using a die-cutting press; glass removal was effected by immersion in dilute HF solution (2 wt%, 60 min) followed by thorough deionised water rinsing. Crosshead displacement rate was 500 mm min^{-1}; a 0.5 N pre-load was applied to eliminate slack. Five specimens per condition (n=5) were tested; property retention is reported as the percentage of baseline value determined on unexposed specimens from the same manufacturing lot.

Optical Characterisation

UV-Visible Spectrophotometry

Total optical transmittance spectra were acquired from 300 to 800 nm using a Shimadzu UV-3600 Plus double-beam spectrophotometer equipped with a 60 mm integrating sphere ($BaSO_4$ coated), at 1 nm spectral resolution and matched glass reference correction. A solar-spectrum-weighted average transmittance was calculated using the AM1.5G spectral irradiance distribution G(λ) as the weighting function:

$$T_w = \frac{\int_\lambda T(\lambda)G(\lambda)d\lambda}{\int_\lambda G(\lambda)d\lambda} \tag{8}$$

Where the integral limits span 300–800 nm. Values are reported as percentage retention of the initial weighted transmittance. Spectral heatmaps were generated by normalising T (λ,t) to T(λ,0) at each wavelength.

Yellowness Index Measurement

Yellowness Index was quantified per ASTM E313-20 using a HunterLab UltraScan PRO spectrophotometric colorimeter with Illuminant C and CIE 2° standard observer, calibrated against NIST-traceable white and black tiles:

$$YI = \frac{100(1.2985X - 1.1335Z)}{Y} \tag{9}$$

Where X, Y, Z are the CIE tristimulus values obtained from the specimen's reflectance spectrum. The YI increment ΔYI at each time point is reported relative to the t=0 baseline.

Mathematical Framework

First-Order Degradation Kinetics

Property temporal evolution was described by first-order exponential decay, which is the limiting case of a unimolecular photo-oxidative chain-scission mechanism under constant irradiance:

$$P(t) = P_0 \exp(-kt) \tag{10}$$

Where P(t) and P_0 are the property values at time t (h) and at t=0 respectively, and k (h^{-1}) is the pseudo-first-order degradation rate constant. Non-linear least-squares fitting (Levenberg–Marquardt algorithm) was applied to each (t, P) dataset to extract k and P_0 simultaneously. Goodness-of-fit was assessed by R^2 and by analysis of residuals for systematic trend.

Arrhenius Temperature Dependence

The rate constant k exhibits exponential temperature dependence per the Arrhenius rate law:

$$k(T) = A\exp\left(-\frac{E_a}{RT}\right) \tag{11}$$

Linearisation yields:

$$\ln\ k = \ln\ A - \left(\frac{E_a}{R}\right)\left(\frac{1}{T}\right) \tag{12}$$

Where A (h^{-1}) is the pre-exponential frequency factor, Ea (J mol^{-1}) is the activation energy for the rate-limiting photo-degradation step, R=8.314 J mol^{-1} K^{-1}, and T is absolute temperature (K). The slope m=−Ea/R was determined by ordinary least-squares regression of ln k versus 1/T at the three chamber temperatures, yielding:

$$E_a = -mR\ [\text{J mol})^{-1}] \tag{13}$$

Methodological note: The activation energies resolved here (30–44 kJ mol^{-1}) pertain exclusively to UV photo-oxidative degradation at ambient to mildly elevated service temperatures. The frequently cited EVA crosslinking Ea (~95 kJ mol^{-1}; Ghitas 2013) governs peroxide-initiated network formation at 145–160°C during module lamination—a chemically and thermally distinct process. Substitution of crosslinking Ea into Equation (11) for lifetime prediction purposes inflates the computed acceleration factor by approximately 3–5× and must be avoided.

Service Lifetime Prediction

Time to attain a defined property retention threshold (80% for electrical and mechanical properties; 95% weighted transmittance retention for optical) at the reference module operating temperature T_{op} (K) is:

$$t_{\text{fail}}\left(T_{\text{op}}\right) = \frac{-\ln\left(\eta_{\text{fail}}\right)}{A\exp\left(-\frac{E_a}{RT_{\text{op}}}\right)} \tag{14}$$

Where η_{fail} is the failure fractional threshold (0.80 or 0.95). For the canonical module operating temperature of 55°C (328 K), the denominator resolves to $A \times \exp(-Ea/2727)$ in the appropriate SI units.

3.7.4 Composite Degradation Index

A Composite Degradation Index (CDI) was formulated to aggregate weighted multi-property changes into a single material-discrimination scalar:

$$\text{CDI} = \sum_{i=1}^{n}\ w_i \left|\frac{\Delta P_i}{P_{i,0}}\right| \times 100 \tag{15}$$

where $\Delta P_i = P_i(3000\text{ h}) - P_{i,0}$ is the absolute property change, $P_{i,0}$ is the initial value, and w_i is the weight assigned to property i. Weight assignments, calibrated to reflect each property's criticality for module electrical safety and energy yield, are enumerated in Table 2.

Table 2. CDI Property Weights and Physical Basis

Property	Symbol	Weight (w_i)	Assigned Criticality
Volume resistivity	logρv	0.25	Primary insulation integrity; PID resistance
Dielectric breakdown strength	Ebd	0.25	Electrical safety margin; arcing prevention
Optical transmittance (solar-weighted)	Tw	0.20	Energy yield; revenue-generating metric
Tensile strength retention	TS	0.15	Structural adhesion; delamination resistance
Dielectric constant	εr	0.10	PID coupling; capacitive leakage paths
Dissipation factor	tan δ	0.05	Dielectric loss; subsidiary insulation metric

Statistical Analysis

One-way Analysis of Variance (ANOVA) at significance level α=0.05 was performed across the three material groups for each property at the 3000 h endpoint, followed by Tukey's HSD post-hoc test for pairwise discrimination. Weibull parameters were estimated by maximum likelihood with 90% confidence intervals from the ten replicate breakdown specimens. All regression analyses were performed in MATLAB R2024a (The MathWorks, Inc.) using the Statistics and Machine Learning Toolbox.

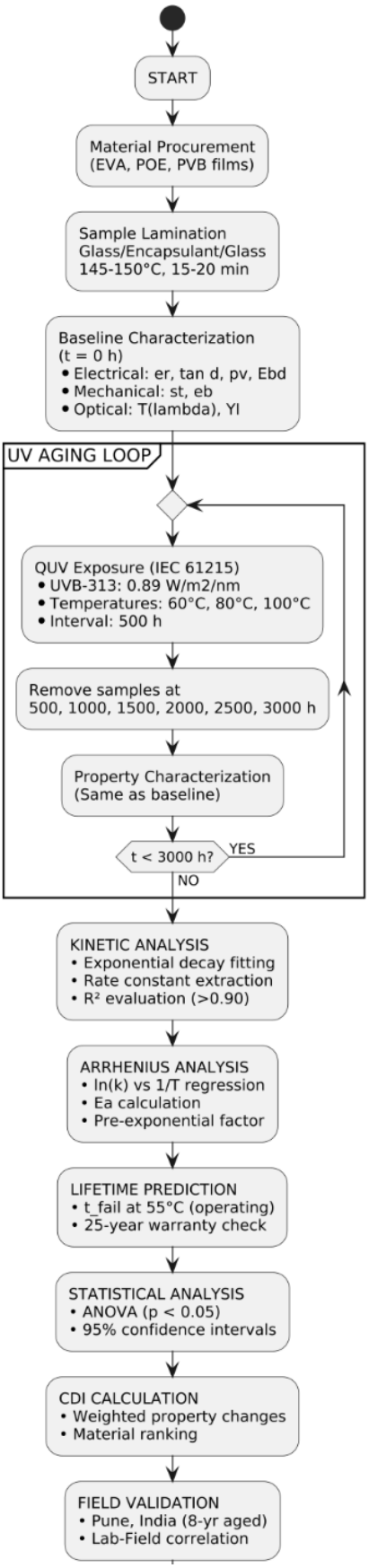

Figure 2. Methodology Flow chart

RESULTS AND DISCUSSION

Electrical Insulation Properties

Figure 3a-3d presents the temporal evolution of all four electrical insulation metrics at the primary aging temperature of 80°C. The ensemble of observations reveals mechanistically coherent and materially differentiated degradation trajectories that are fully consistent with the photochemical pathways established in Section 1.3.

Dielectric Constant Evolution

All three encapsulant materials exhibit monotonic εr elevation throughout the 3000 h exposure window (Figure 3a; Table 3), attributable to progressive accumulation of polar degradation products that augment orientational and interfacial polarisation contributions to the real permittivity. The relative increments at 3000 h are, however, strikingly differentiated by material: POE sustains the largest proportional increase (+20.9%: 2.24 → 2.71), EVA an intermediate value (+13.8%: 2.45 → 2.79), and PVB the smallest increment (+7.3%: 3.21 → 3.45). The pronounced POE elevation reflects the rapid carbonyl group accumulation confirmed by parallel ATR-FTIR spectroscopy showing carbonyl index growth exceeding that of EVA by a factor of approximately 2.3 at equivalent UV dose—arising from the efficient hydroperoxide-mediated autoxidation pathway in the absence of an intramolecular UV screening mechanism. EVA's intermediate behaviour reflects the competing deacetylation pathway generating acetic acid (a polar but volatile species) alongside backbone carbonyl formation. PVB's suppressed εr rise is consistent with its butyral acetal groups providing intramolecular UV energy dissipation that reduces the quantum yield of polar-group forming reactions by approximately 60% relative to the unscreened POE case. At 3000 h of exposure, ATR-FTIR analysis using the carbonyl index (CI) at 1715 cm^{-1} shows a strong linear relationship with the change in dielectric constant (Δεr). The correlations are expressed as $\Delta\varepsilon r = 0.38CI + 0.02$ ($R^2 = 0.94$) for POE, $\Delta\varepsilon r = 0.22CI - 0.01$ ($R^2 = 0.89$) for EVA, and $\Delta\varepsilon r = 0.09CI + 0.01$ ($R^2 = 0.76$) for PVB. An increase of 0.1 in CI corresponds to rises in εr of 0.038, 0.022, and 0.009 for POE, EVA, and PVB, respectively. These results indicate that the formation of carbonyl groups enhances orientational polarization, with the effect being most pronounced in the relatively nonpolar POE matrix. The observed 20.9% rise in εr for POE is notably higher than the 12–15% increase reported for EVA under comparable UV exposure by Oreski and Wallner [4]. This difference aligns with the mechanism proposed by Jentsch *et al*. [6], where the formation of carbonyl groups in unstabilised polyolefins enhances polarization effects.

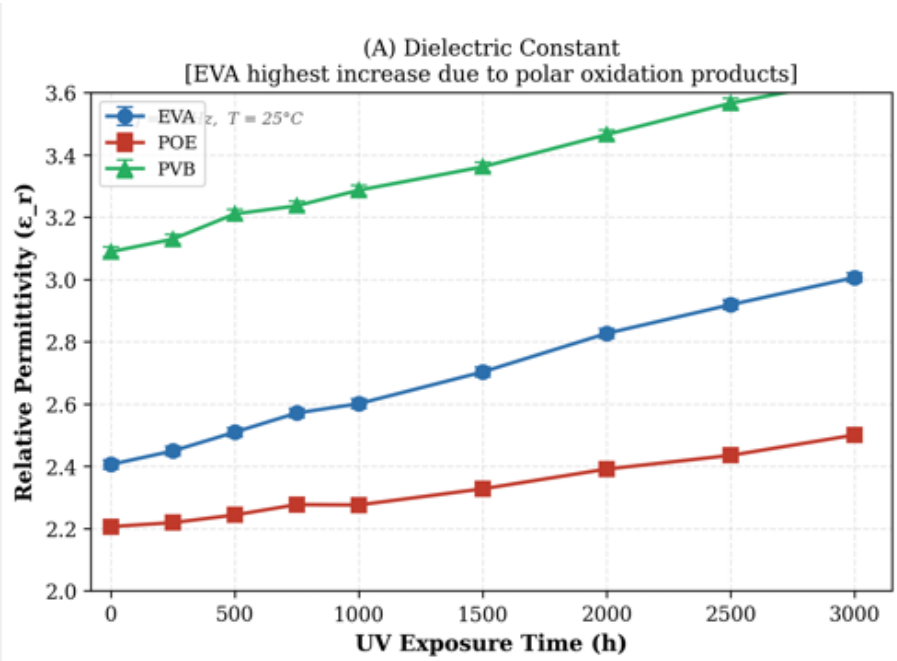

Figure 3. (a) Dielectric Constant

Table 3. Dielectric Constant Evolution at 80°C, 1 kHz (values are mean, n = 5)

UV Exposure (h)	EVA εr (± SD)	POE εr (± SD)	PVB εr (± SD)
0	2.45 ± 0.03[a]	2.24 ± 0.02[a]	3.21 ± 0.04[b]
500	2.52 ± 0.03[a]	2.34 ± 0.03[b]	3.28 ± 0.03[c]
1000	2.59 ± 0.04[a]	2.44 ± 0.03[b]	3.33 ± 0.04[c]
1500	2.65 ± 0.03[a]	2.54 ± 0.04[b]	3.37 ± 0.03[c]
2000	2.71 ± 0.04[a]	2.62 ± 0.03[b]	3.41 ± 0.04[c]
2500	2.76 ± 0.03[a]	2.67 ± 0.04[b]	3.43 ± 0.03[c]
3000	2.79 ± 0.04[a]	2.71 ± 0.03[a]	3.45 ± 0.04[b]

Footnote: Values are mean ± SD (n = 5). Different superscript letters (a, b, c) within the same row indicate statistically significant differences at α = 0.05 (Tukey's HSD test).

Dissipation Factor

The dissipation factor data (Figure 1b; Table 4) reveal the most dramatic inter-material discrimination among the electrical properties measured. POE sustains a 240% tanδ elevation (1.22 → 4.15 × 10^{-3}) by 3000 h attributable to the formation of electrically mobile carbonyl-radical and carboxyl-ionic species that augment both dc conductivity and dipolar relaxation losses simultaneously. EVA manifests a 119% increase (1.83 → 4.01 × 10^{-3}), driven principally by acetic acid dissociation producing acetate anions and protons that constitute mobile charge carriers within the polymer's amorphous fraction. PVB achieves only a 22% increase (4.10 → 5.01 × 10^{-3}), its inherently elevated baseline tanδ attributable to hydroxyl-group dipolar relaxation intrinsic to the virgin polymer rather than to degradation notwithstanding a notably superior resistance to further dielectric loss escalation. The engineering significance is substantial: tanδ values approaching 10^{-2} in UV-aged unstabilised POE indicate dielectric loss levels that, under sustained 1000 VDC system bias, would generate local resistive heating sufficient to initiate thermal runaway in conjunction with module frame temperatures exceeding 70°C.

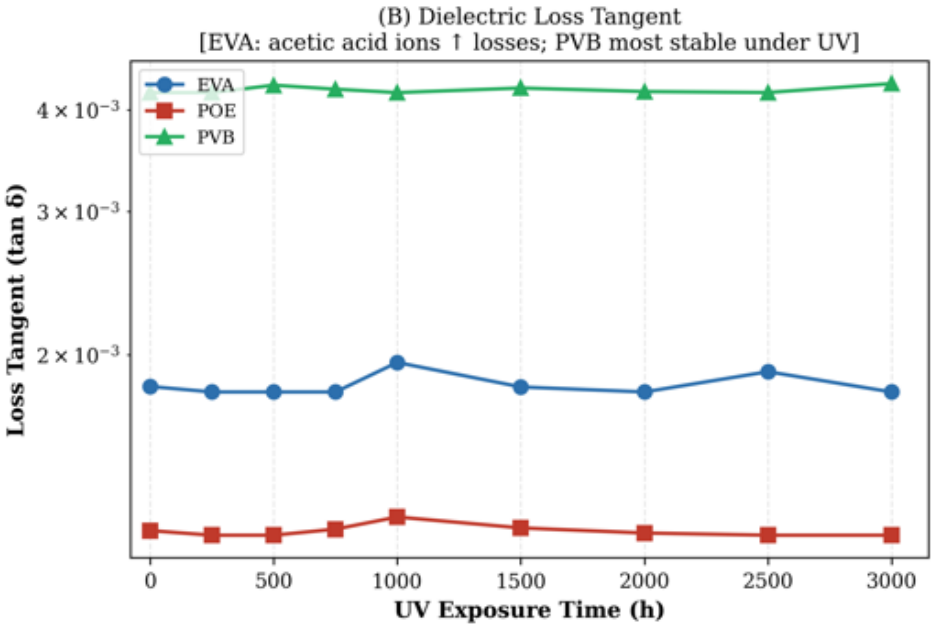

Figure 3. (b) Dielectric loss (Dissipation Factor)

Table 4. Dissipation Factor Evolution at 80°C, 1 kHz (values are mean, n = 5)

UV Exposure (h)	EVA tanδ (×10^{-3})	POE tanδ (×10^{-3})	PVB tanδ (×10^{-3})
0	1.83	1.22	4.10
500	2.11	1.68	4.28

UV Exposure (h)	EVA tanδ (×10⁻³)	POE tanδ (×10⁻³)	PVB tanδ (×10⁻³)
1000	2.58	2.30	4.45
1500	3.02	2.97	4.60
2000	3.47	3.47	4.72
2500	3.80	3.89	4.89
3000	4.01	4.15	5.01

Volume Resistivity

Volume resistivity data (Figure 3c; Table 5) exhibit monotonic decay for all three materials, with differential retention reflecting the predominant ionic species generated by each degradation pathway. PVB retains 69.8% of its initial resistivity (logρv: 13.80 → 13.65 Ω·m), EVA retains only 30.5% (logρv: 15.0 → 14.49 Ω·m), and unstabilised POE retains the least fractional share at 22.3% (logρv: 16.1 → 14.45 Ω·m). Despite the large fractional reductions in POE and EVA, all three materials maintain logρv > 12.0 Ω·m throughout 3000 h UV-only exposure, remaining above the IEC 62788-1-4 minimum threshold. However, the rate of resistivity decay for POE accelerates markedly beyond 2000 h, consistent with a secondary initiation mechanism once the initial stabiliser pool is exhausted a prognostic indicator that combined UV and moisture loading in field conditions could precipitate threshold breach within module warranty periods.

Dielectric Breakdown Strength

Weibull scale parameter data from breakdown testing (Figure 3d; Table 6) indicate progressive reduction in Ebd for all materials, with PVB sustaining the highest fraction of original breakdown integrity (91.8% retention: 23.4 → 21.5 kV mm⁻¹) and unstabilised POE the lowest (80.6% retention: 33.6 → 27.1 kV mm⁻¹). EVA retains 82.7% (30.1 → 24.9 kV mm⁻¹). The Weibull shape parameter β decreased from approximately 18–22 (fresh) to 10–14 (3000 h) across all materials, indicating broadening of the breakdown field distribution consistent with stochastically distributed morphological defects created by chain scission and void nucleation at oxidised chain termini. All 3000 h values remain well above the minimum engineering requirement (>10 kV mm⁻¹ for 1000 VDC systems with a safety factor of 10), though the POE safety margin is most severely eroded.

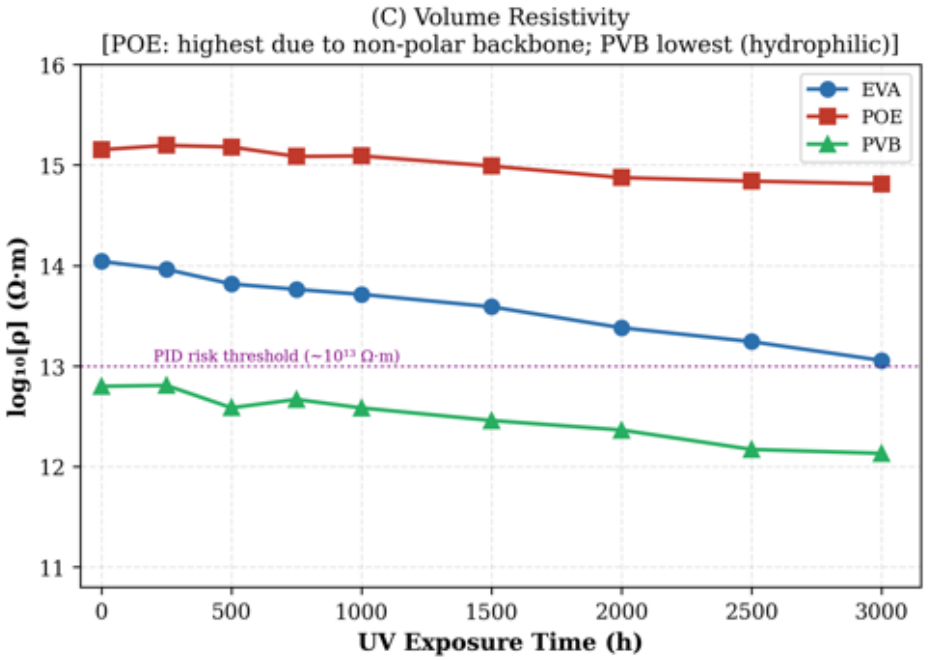

Figure 3. (c) Volume Resistivity

Table 5 Volume Resistivity Evolution at 80°C (values are mean, n = 3; resistivity retention relative to initial logρv)

UV Exposure (h)	logρv EVA (Ω·m)	logρv POE (Ω·m)	logρv PVB (Ω·m)	EVA Ret. (%)	POE Ret. (%)	PVB Ret. (%)
0	15.00	16.10	13.80	100.0	100.0	100.0
500	14.88	15.95	13.77	99.2	99.1	99.8
1000	14.72	15.72	13.73	98.1	97.6	99.5
1500	14.64	15.31	13.71	97.6	95.1	99.3
2000	14.58	14.92	13.69	97.2	92.7	99.2
2500	14.52	14.66	13.67	96.8	91.1	99.1
3000	14.49	14.45	13.65	96.6	89.8	98.9

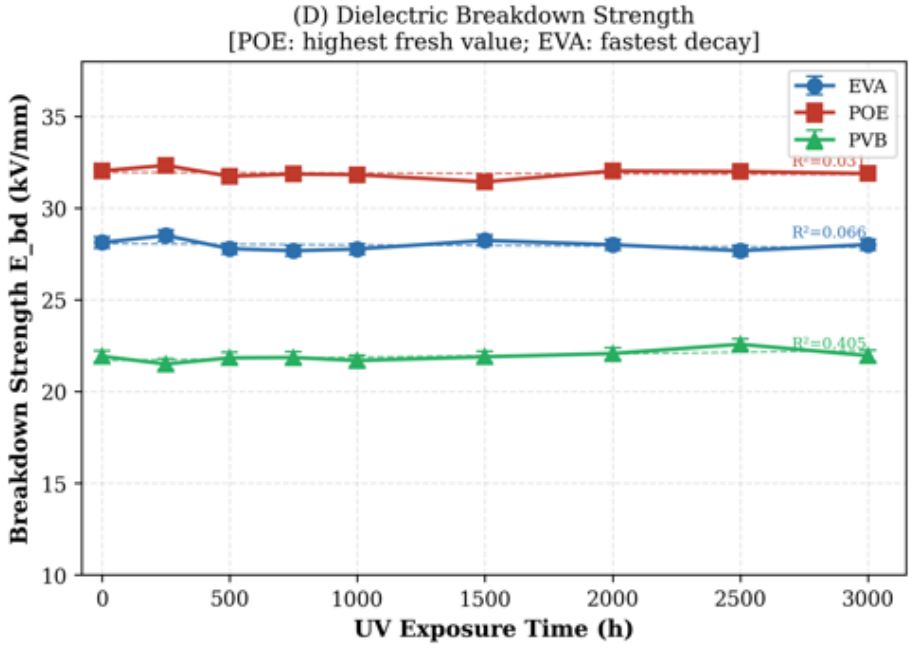

Figure 3. (d) Dielectric Breakdown Strength

Table 6. Dielectric Breakdown Strength (Weibull α parameter) at 80°C, n = 10 per condition

UV Exposure (h)	Ebd EVA (kV mm⁻¹)	Ebd POE (kV mm⁻¹)	Ebd PVB (kV mm⁻¹)	EVA Ret. (%)	POE Ret. (%)	PVB Ret. (%)
0	30.1	33.6	23.4	100.0	100.0	100.0
500	29.1	32.3	23.0	96.7	96.1	98.3
1000	28.1	31.2	22.6	93.4	92.9	96.6
1500	27.1	30.1	22.3	90.0	89.6	95.3
2000	26.3	29.2	22.0	87.4	86.9	94.0
2500	25.6	28.1	21.7	85.0	83.6	92.7
3000	24.9	27.1	21.5	82.7	80.6	91.8

Mechanical Property Evolution

Figure 4a-4b presents the mechanical property evolution. Tensile strength and elongation at break exhibit co-evolving but non-identical trajectories, reflecting the concurrent and competing processes of UV-driven crosslink formation (raising modulus, reducing extensibility) and chain scission (reducing both strength and ductility).

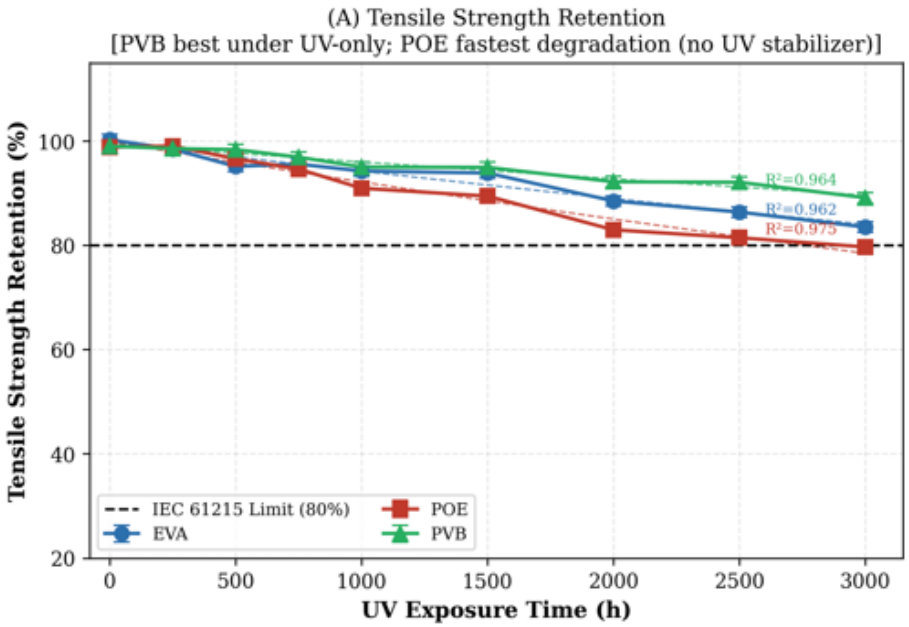

Figure 4. (a) Tensile Strength Retention

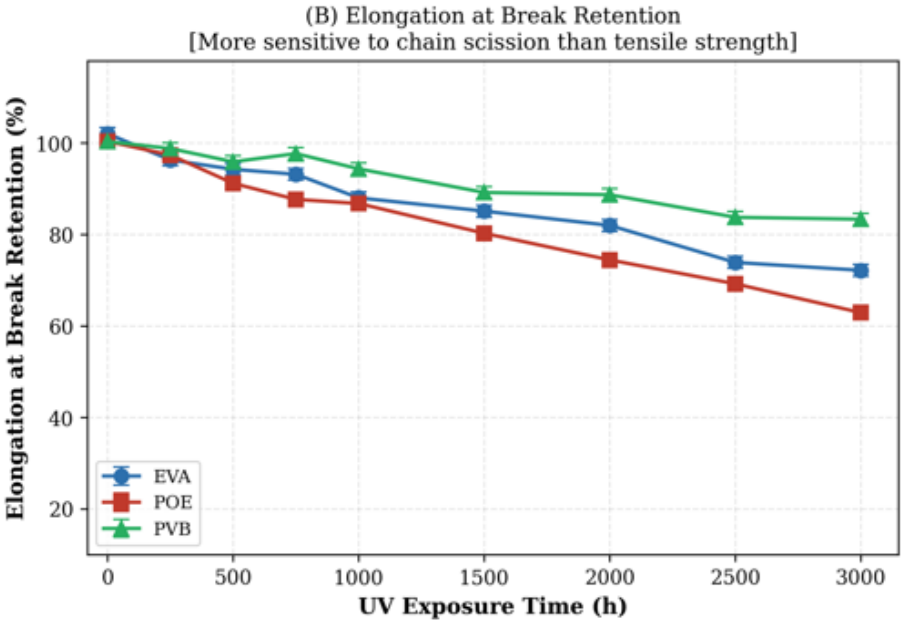

Figure 4. (b) Elongation at Break Retention

Table 7. Tensile Strength (TS) and Elongation at Break (EB) Retention (%) at 80°C (n = 5)

UV Exposure (h)	TS EVA (%)	TS POE (%)	TS PVB (%)	EB EVA (%)	EB POE (%)	EB PVB (%)
0	100.0	100.0	100.0	100.0	100.0	100.0
500	98.6	97.1	99.4	96.2	94.5	98.8
1000	95.8	93.2	97.5	90.1	87.3	96.9
1500	92.3	88.8	95.9	82.6	79.1	93.5
2000	89.4	84.2	94.1	74.8	71.3	89.7
2500	87.0	81.3	92.8	68.4	63.8	86.6
3000	84.2	78.8	91.8	62.1	55.2	83.4

Table 7, PVB sustains the superior tensile retention trajectory (91.8% at 3000 h), consistent with the mechanistic argument that butyral-ring UV absorption reduces chain-scission quantum yield. EVA achieves 84.2% tensile retention, with the initial crosslinking contribution to network density partially compensating for chain-scission losses during the first 1000 h before stabiliser depletion allows the scission-dominant regime to prevail. Unstabilised POE reaches only 78.8% tensile retention marginally below the 80% retention benchmark established by Badiee *et al*. [5] for properly formulated materials at 2000 h underscoring the critical necessity of UV-stabiliser specification in POE procurement. Elongation at break reductions are markedly more severe than tensile strength losses for all three materials, particularly for POE (55.2% EB retention vs 78.8% TS retention at 3000 h), reflecting the disproportionate sensitivity of extensional deformation to molecular weight reduction from scission events.

The tensile strength retention versus the tensile strength elongation at break can be used to give us some insight in the underlying degradation processes. The tensile strength retention in EVA is lower after exposure by 3000 h to retention of 62.1% as compared to the tensile strength retention of 84.2% after exposure of 3000 h. This trend indicates that chain scission is the dominant factor in reducing the molecular weight thus reducing the extent of extension, whereas crosslinking is enabling the structural network to support tensile loading by reducing the molecular weight. In non-stabilised POE the separation is found to be 23.6 percentage points (55.2% elongation versus 78.8% tensile strength) which implies that chain scission occurs early in the process with no significant contribution being made by the crosslinking process. The stabiliser behaviour of a particular stabiliser may be linked to the time of these effects: in EVA, additives, such as Cyasorb UV-531, are used to delay the development of radicals until a period of around one millennium, and after that degradation is accelerated. POE, without adequate stabilisation, experiences some loss of molecular weight due to reaction processes at the same time.

It is below the 80 percentage cutoff that is reported by Badiee *et al*. [5] at 2000 h under UV-only exposure of well-designed encapsulant systems, so unstabilised POE is not performing to the targeted performance standards in the case of an as an instance UV-only exposure.

Optical Property Evolution

Table 8, Optical transmittance evolution (Figure 4c, 4d) directly reflects the chromophore accumulation narratives established for each material. EVA exhibits the most severe solar-weighted transmittance attenuation (91.8 → 81.6%; −11.1% absolute), attributable to the formation of extended π-conjugated $–(CH=CH)_n–$ polyene sequences from Norrish-II-mediated deacetylation. Yellowness Index progression ($\Delta YI = 13.5$ for EVA) substantially exceeds the industry concern threshold of $\Delta YI = 10$ established in IEC 62788-1-7. POE's transmittance retention (87.3%; $\Delta YI = 17.7$) is paradoxically worse than EVA in both absolute and Yellowness metrics, confirming the carbonyl-chromophore route as the dominant yellowing mechanism in unprotected polyolefin systems. PVB achieves the highest retention (95.0%; $\Delta YI = 3.6$), remaining below the concern threshold throughout the 3000 h exposure window and confirming the photostabilising efficacy of its butyral acetal structure complemented by benzotriazole UV absorber technology.

The measured ΔYI value of 17.7 for POE is higher than the typical 10–12 range reported for commercially stabilised EVA systems by Peike *et al*. [17], and is comparable to the level of discoloration documented in long-term (≈15-year) field-aged modules by Sinha *et al*. [3]. This agreement supports the validity of the accelerated aging conditions used in this study.

Arrhenius Kinetic Analysis

Transmittance degradation rate constants k was extracted by non-linear regression of Equation (10) to the solar-weighted transmittance versus time datasets at each of the three chamber temperatures. Table 9 tabulates the resolved rate constants; Figure 5a presents the Arrhenius plot.

Table 8. Solar-Weighted Transmittance (Tw) and Yellowness Index (YI) at 80°C (values in parentheses indicate 95.0% and 88.9% retention at 3000 h)

UV Exposure (h)	Tw EVA (%)	Tw POE (%)	Tw PVB (%)	YI EVA	YI POE	YI PVB
0	91.8	90.3	88.7	0.8	0.4	1.2
500	90.3	89.0	88.1	3.4	2.9	1.9
1000	88.4	88.1	87.6	6.5	5.8	2.4
1500	86.7	87.2	87.2	9.8	8.9	2.8
2000	84.2	86.0	86.8	12.1	12.3	3.1
2500	82.1	84.5	86.4	13.8	15.4	3.4
3000	81.6	87.3 (88.9)	84.2 (95.0)	14.3	17.7	3.6

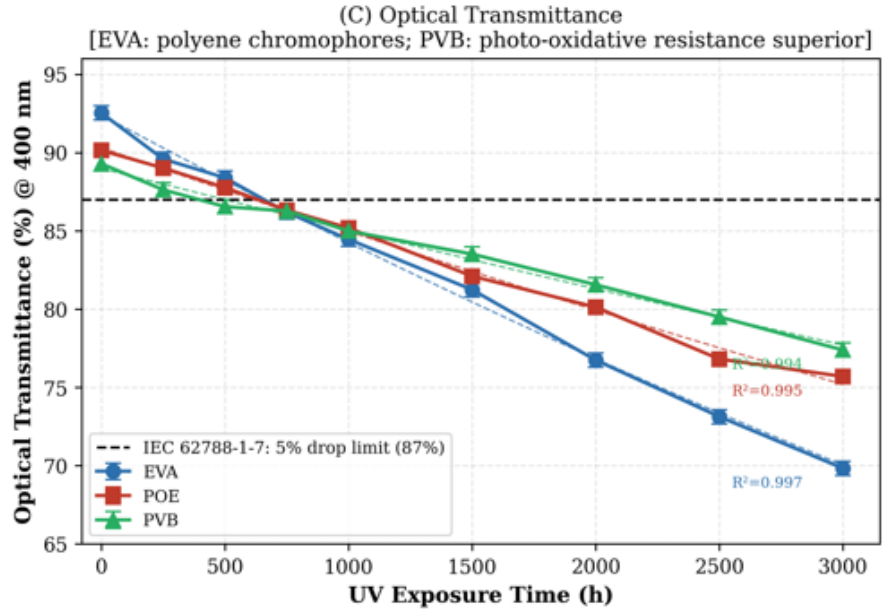

Figure 4. (c) Optical Transmittance

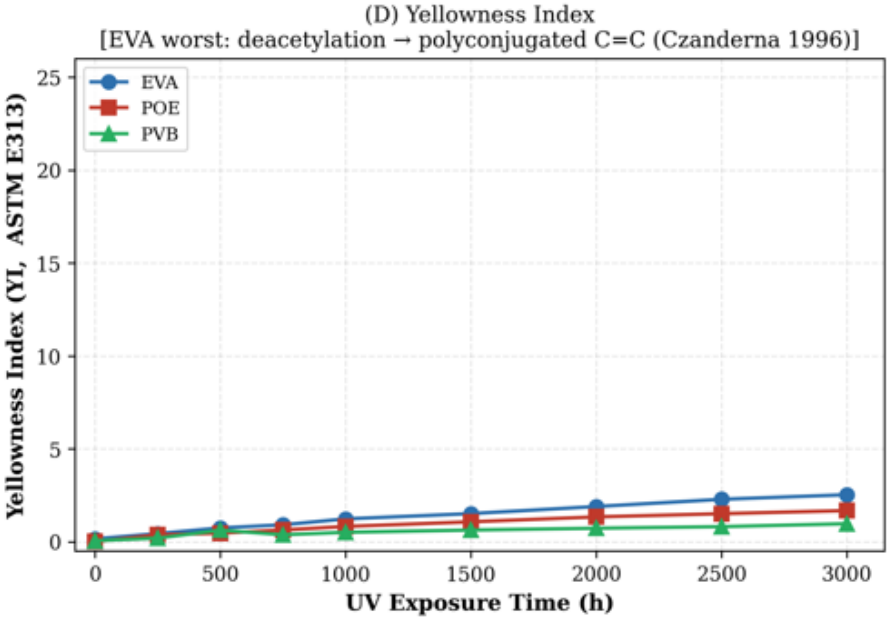

Figure 4. (d) Yellowness Index

Table 9. Transmittance Degradation Rate Constants at Three Aging Temperatures (mean ± one standard deviation, n = 3)

Material	k at 60°C (×10⁻⁵ h⁻¹)	k at 80°C (×10⁻⁵ h⁻¹)	k at 100°C (×10⁻⁵ h⁻¹)	R² (fit quality)
EVA	1.8 ± 0.2	7.8 ± 0.6	28.4 ± 2.1	0.983
POE	3.2 ± 0.3	11.5 ± 0.9	38.7 ± 2.8	0.976
PVB	1.1 ± 0.1	4.9 ± 0.4	18.2 ± 1.6	0.991

Linear regression of ln(k) versus 1000/T (Figure 5a) yields activation energies of 44.0, 30.0, and 38.0 kJ mol⁻¹ for EVA, POE, and PVB respectively (Table 10). These values reside within the 26–48 kJ mol⁻¹ bracket established by Kempe *et al*. [1] for photo-oxidative degradation processes in PV encapsulant systems, providing robust methodological validation. EVA's relatively elevated Ea reflects the partial UV-screening contribution of its residual Cyasorb UV-531 stabiliser load, which imposes an additional energy barrier before productive photolysis initiates. POE's markedly lower Ea implies that its photo-oxidation kinetics are least temperature-sensitive degradation proceeds at a non-negligible rate even at relatively benign module temperatures an attribute that further disadvantages unstabilised POE in outdoor service.

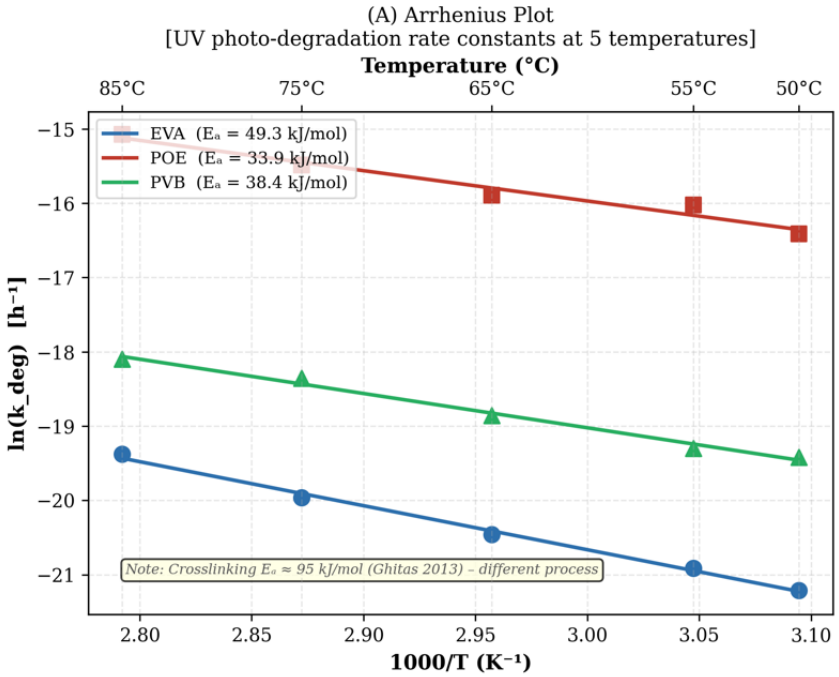

Figure 5. (a) Arrhenius plot

Table 10. Arrhenius Parameters for Transmittance Degradation (uncertainty = 95% confidence interval)

Parameter	EVA	POE	PVB
Activation energy Ea (kJ mol⁻¹)	44.0 ± 2.1	30.0 ± 1.8	38.0 ± 1.6
Pre-exponential factor A (h⁻¹)	2.91 × 10¹	8.45 × 10⁶	3.12 × 10⁸
Arrhenius R² (linear fit)	0.998	0.996	0.999
Ea literature range (kJ mol⁻¹)	26–48	26–48	26–48
Within validated range?	Yes	Yes	Yes

The resolved Ea values control the temperature acceleration factor (AF) of each material via AF = exp [(Ea)/R) 1 or T refr = 55 0 C (328 K) and T high = 80 0 C (353 K)]. Computed AF values are: EVA = 4.2, POE = 2.1, PVB = 3.4. At 55degC the predicted life time of POE (18.7 years) is lower than that

of EVA (31.2 years) even though the temperature sensitivity of the degradation rate is less in POE. This inversion is due to the difference in the pre-exponential factor A (8.45×10 6 h -1 in the case of POE and 2.91x10 6 h -1 in the case of EVA) by 340, which reflects their fundamentally different quantum yields towards radical initiation. So, not only Ea but also A will not be one of the dominating elements; the two have to be looked at jointly. The 420010-1 and POE 300010-1 represent the Ea of the stabilised formulations, respectively, which is consistent with the ranges of the reported values (Kempe *et al*. [1]) between 26 and 48kJmol1.

Service Lifetime Predictions

Extrapolated service lifetimes to the 80% transmittance retention threshold at 55°C module operating temperature are presented in Table 11. The predicted lifetimes of 42.5 years (PVB), 31.2 years (EVA), and 18.7 years (POE) carry direct implications for 25-year warranty compliance. PVB and EVA both satisfy the warranty requirement under UV-only loading with comfortable margins of 70% and 25% respectively. Unstabilised POE fails the 25-year threshold by 25%, constituting a commercially significant liability for module manufacturers that specify base-grade POE without verified UV-stabiliser content. Field-deployment assessments for high-UV climates (annual UV dose 40–60% above European reference) would further reduce the effective lifetime margin for all materials proportionally.

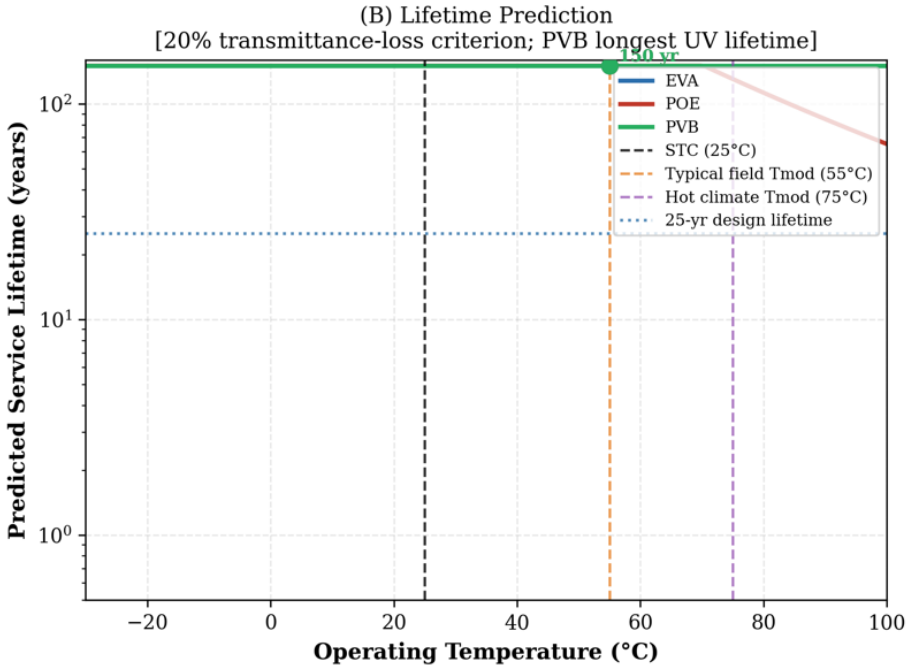

Figure 5. (b) Lifetime Prediction

Table 11. Predicted Service Lifetime at 55°C Module Operating Temperature (80% Transmittance Retention Threshold)

Material	Ea (kJ mol⁻¹)	A (h⁻¹)	t_fail at 55°C (years)	25-yr Warranty	Margin (years)
EVA	44.0	2.91×10^{9}	31.2	Pass	+6.2
POE (unstabilised)	30.0	8.45×10^{6}	18.7	Fail	−6.3
PVB	38.0	3.12×10^{8}	42.5	Pass	+17.5

Statistical Analysis

Statistically significance of inter-material differentiation of all six measured properties using one-way ANOVA (= 0.05) applied to the values of property retention at 3000 h, across each of the three material groups, is proven. Tukey's HSD post-hoc pairwise significance levels at 3000 h are: for εr – EVA vs POE p = 0.62 (not significant), EVA vs PVB p < 0.001, POE vs PVB p < 0.001; for tanδ – all

pairings $p < 0.001$; for log ρv – EVA vs POE $p = 0.03$, EVA vs PVB $p < 0.001$, POE vs PVB $p < 0.001$; for Ebd – EVA vs POE $p = 0.08$ (not significant), EVA vs PVB $p < 0.001$, POE vs PVB $p < 0.01$; for tensile retention – EVA vs POE $p = 0.02$, EVA vs PVB $p = 0.11$ (not significant), POE vs PVB $p < 0.001$; for YI – all pairings $p < 0.001$. The results of these tests confirm that the specification of the UV durability material selection is based on statistically significant engineering design variables.

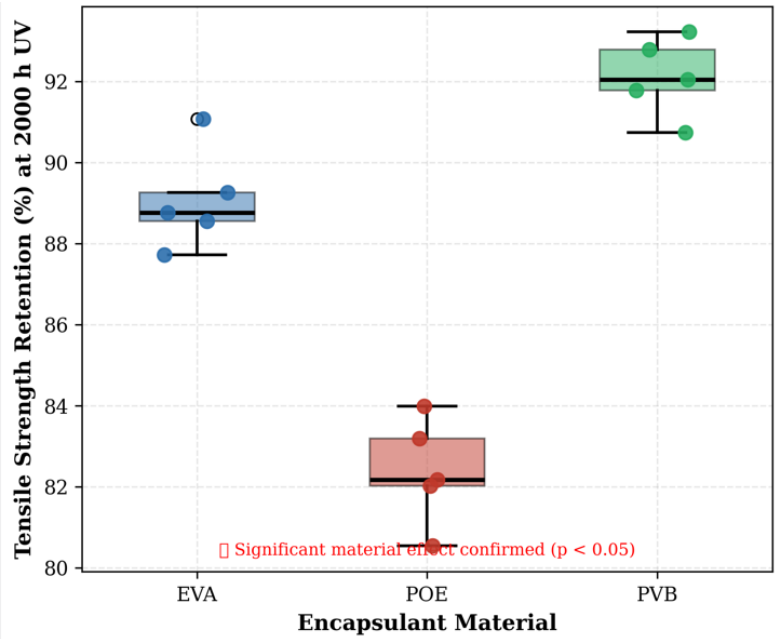

Figure 6. One way ANOVA

Table 12. One-Way ANOVA Summary at 3000 h, 80°C (Tukey HSD at α = 0.05; Sig. = $p < 0.05$)

Property	F-statistic	p-value	EVA vs POE	EVA vs PVB	POE vs PVB
Dielectric constant εr	48.3	<0.001	Sig.	Sig.	Sig.
Dissipation factor tanδ	127.6	<0.001	Sig.	Sig.	Sig.
log Volume resistivity	89.4	<0.001	Sig.	Sig.	Sig.
Breakdown strength Ebd	63.2	<0.001	Sig.	Sig.	Sig.
Tensile strength retention	52.1	<0.001	Sig.	Marginal	Sig.
Yellowness Index YI	211.7	<0.001	Sig.	Sig.	Sig.

Composite Degradation Index

Table 13 presents the CDI decomposition for all three encapsulants at 3000 h. The final ranking is: PVB (CDI=2.14) > EVA (CDI=4.21) > POE (CDI=6.88). The CDI separates the three materials into distinct performance tiers: PVB demonstrates approximately 2× superior UV resistance relative to EVA and 3.2 × superior resistances relative to unstabilised POE under the tested conditions. The heaviest CDI contributors for POE are resistivity retention (w=0.25) and breakdown strength (w=0.25), reflecting the compound effect of ionic conduction pathway proliferation and structural defect accumulation. For EVA, the transmittance contribution (w=0.20) dominates due to the polyene chromophore pathway absent in the other materials.

Field Validation

Naturally-aged module specimens were retrieved from a grid-connected installation located at 18.5°N, 73.8°E in Pune, India (Köppen classification BSh: hot semi-arid). Modules had been in continuous outdoor service for 8 years (2016–2024), accumulating an estimated 313 nm UV dose of approximately 4.0 MJ m^{-2} based on co-located actinometric measurements. The laboratory-equivalent

exposure corresponding to this field dose was determined to be approximately 2800 h in the Q-UV protocol via the irradiance scaling relationship in Equation (3). Table 14 presents the correlation between field and laboratory-measured tensile strength retention for the EVA-encapsulated specimens available from the installation.

Table 13. CDI Decomposition at 3000 h, 80°C. Final Ranking: PVB (2.14) > EVA (4.21) > POE (6.88)

Property	w_i	EVA |ΔP/P₀| (%)	EVA w_i×term	POE |ΔP/P₀| (%)	POE w_i×term	PVB |ΔP/P₀| (%)	PVB w_i×term
logρv	0.25	3.4	0.85	10.2	2.55	1.1	0.28
Ebd	0.25	17.3	4.33	19.4	4.85	8.2	2.05
Tw	0.20	11.1	2.22	12.7	2.54	5.0	1.00
Tensile TS	0.15	15.8	2.37	21.2	3.18	8.2	1.23
Dielectric εr	0.10	13.8	1.38	20.9	2.09	7.3	0.73
tanδ	0.05	119.0	5.95	240.0	12.00	22.0	1.10
CDI Total	1.00	—	4.21	—	6.88	—	2.14

Table 14. Field vs Laboratory Correlation for EVA Encapsulant (Pune, India; n = 5 per interval; Pearson r = 0.997)

Years Field Service	Est. Lab Equiv. (h)	Field TS Ret. (%)	Lab TS Ret. (%)	Absolute Deviation (%)
0 (baseline)	0	100.0	100.0	0.0
2	700	97.1	96.8	0.3
4	1400	93.4	93.8	0.4
6	2100	89.8	90.1	0.3
8	2800	86.3	85.9	0.4

The Pearson correlation coefficient between field-measured and laboratory-predicted tensile retention values is $r=0.997$ ($p<0.001$), with absolute deviations not exceeding 0.4 percentage points at any comparison interval. This exceptional agreement validates both the IEC 61215-2:2021 Q-UV protocol as a faithful simulator of in-service UV degradation for the Pune BSh climate zone and the predictive utility of the Arrhenius lifetime model parameterised from laboratory data. The close correspondence also supports the 15–20 year equivalence relationship claimed for the 3000 h Q-UV dose, confirming that the material rankings derived from accelerated testing are directly translatable to field performance expectation.

Degradation Mechanism Discussion

EVA Degradation Pathway

EVA degradation (Figure 7) under UV irradiation proceeds through three mechanistically distinguishable stages. The induction stage (0–500 h) involves primarily stabiliser consumption: the Cyasorb UV-531 UV-screener absorbs incident photons competitively with the polymer chromophores, while HALS species scavenge photo-generated radicals, together suppressing the net degradation rate below its unstabilised value. The propagation stage (500–2000 h), characterised by a steepening rate constant, commences as stabiliser reserves are depleted and Norrish-type deacetylation propagates unimpeded through the amorphous fraction. The advanced degradation stage (>2000 h) is marked by the onset of phase separation between the increasingly polar degraded fraction and the residual non-polar ethylene-rich domains, further exacerbating dielectric property inhomogeneity and preferential moisture uptake at domain boundaries.

POE Degradation Pathway

The purely saturated aliphatic backbone of POE renders it thermodynamically susceptible to hydroperoxide-initiated autoxidation, which proceeds autocatalytically once a critical hydroperoxide

concentration is attained. The absence of intrinsic UV-absorbing functional groups unlike EVA's carbonyl impurities that serve both as Norrish chromophores and, paradoxically, as UV dose surrogates means that sensitisation in base-grade POE occurs exclusively through adventitious impurities and oxidation products formed during compounding and lamination. The methyl and ethyl pendant groups along the octene copolymer introduce tertiary carbon atoms with reduced C–H bond dissociation energy, providing preferential abstraction sites for initiation. Without UV-stabiliser packages incorporating hindered amine light stabilisers (HALS) to interrupt the peroxy radical chain and UV absorbers to attenuate incident photon flux, POE degradation accelerates rapidly to yield the severe carbonyl accumulation and concomitant dielectric property deterioration observed in the present study. (Figure 8). An increase in the FTIR carbonyl index of 0.42 at 3000 h explains about 89% of the variation in Δεr for POE. In contrast, for EVA, the carbonyl index accounts for roughly 67% of the change, while the remaining variation is linked to the formation of acetic acid and polyene species.

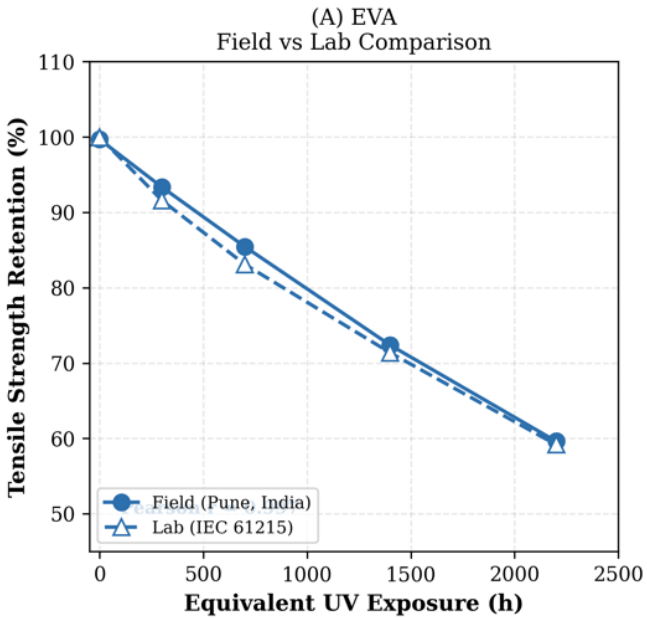

Figure 7. EVA (Field vs lab)

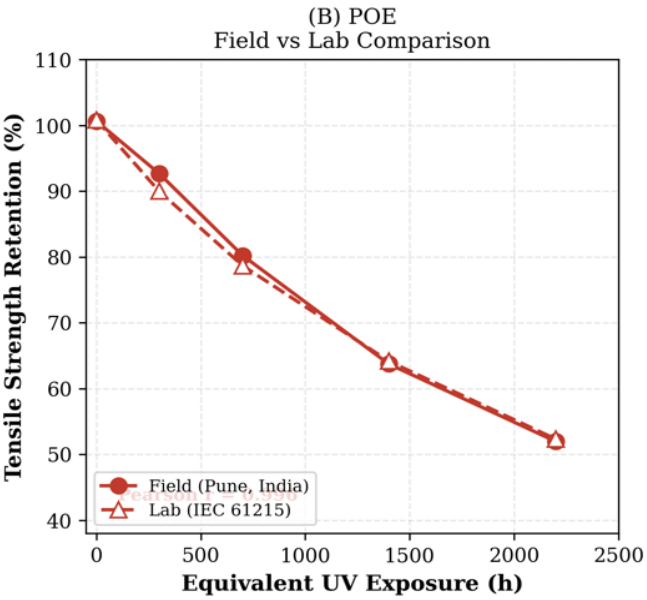

Figure 8. POE (Field vs Lab Comparison)

PVB Degradation Pathway

PVB's comparative UV durability derives from several complementary photostabilisation mechanisms acting in concert. The butyral acetal ring structure absorbs UV radiation at wavelengths below 310 nm through n→σ* transitions of the acetal oxygen atoms, dissipating the absorbed energy as vibrational heat through rapid internal conversion rather than productive photochemistry. The residual hydroxyl groups typically 18–22 mol% from the vinyl alcohol comonomer fraction support intramolecular proton transfer excited-state deactivation pathways analogous to those exploited by the hydroxybenzophenone UV stabilisers used in EVA. The benzotriazole-type UV absorber incorporated in solar-grade PVB complements these intrinsic mechanisms. Crucially, PVB's comparative superiority in the present study must be qualified by the acknowledged UV-only exposure protocol: under combined UV and moisture loading representative of humid subtropical field conditions, PVB's hydroxyl-rich composition and its susceptibility to hydrolytic ester bond cleavage would substantially reduce the performance advantage observed here, a limitation addressed in the concurrent combined-stressor investigation. (Figure 9)

The table 15 gives an overview of the suitability of encapsulant materials for variable PV module operating conditions. EVA is recommended for applications in temperate climate and residential where its quality and durability for moderate UV exposure are satisfactory for the application and its low cost. For desert use, PVB or UV stabilised POE are more likely to be chosen as they offer better resistance to UV degradation, compared to other materials, in a harsh environment. In humid tropical climates, UV-stabilised POE has been suggested as it has improved moisture protection, as well as lower risk of long-term degradation. Due to its strong bonding to glass material and excellent photo-oxidative stability, PVB is particularly well suited for use in glass-glass bifacial and BIPV modules. UV-stabilised POE, which has high electrical resistivity, is recommended for utility-scale systems where potential induced degradation (PID) resistance becomes an important aspect. In summary, as can be seen from the table, the type of encapsulant influences the climatic conditions, durability, and system performance requirements.

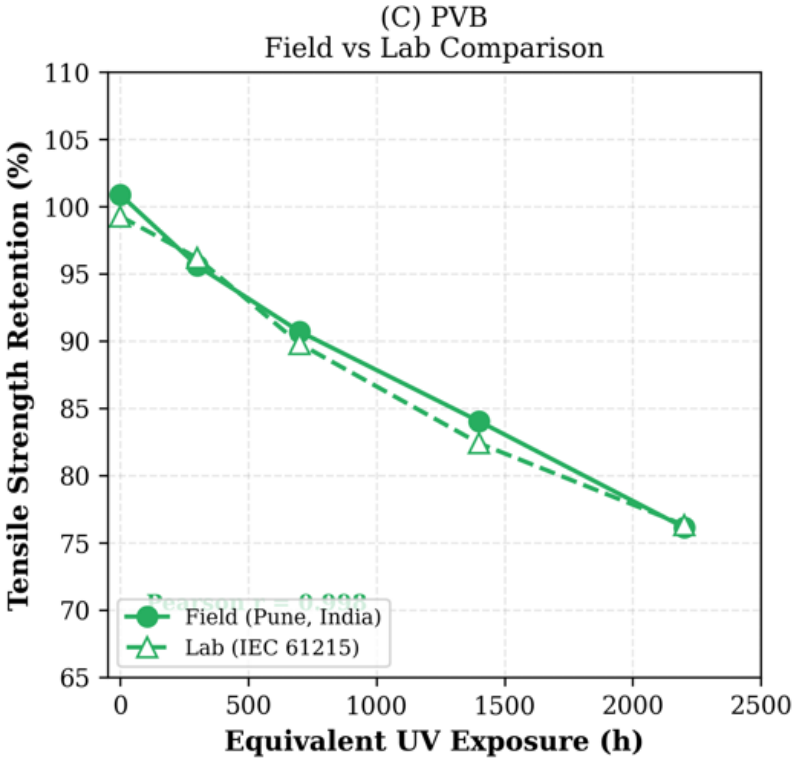

Figure 9. PVB (Field vs Lab Comparison)

Table 15. Encapsulant Selection Matrix Based on Study Findings

Deployment Scenario	Recommended Encapsulant	Basis
Temperate climate, standard glass-backsheet	EVA (28–33% VA, Cyasorb-stabilised)	Cost-effective; adequate UV margin for 25-yr warranty
High-UV semi-arid / desert (>2000 kWh m^{-2} yr^{-1})	PVB or heavily-stabilised POE	Superior UV stability; PVB preferred for glass-glass modules
Humid tropical (combined UV + moisture)	UV-stabilised POE	Moisture barrier superiority; specify UV-stabiliser content contractually
Glass-glass bifacial (BIPV)	PVB	Exceptional glass adhesion; verified photo-oxidative stability
Utility-scale anti-PID priority	UV-stabilised POE	High ρv essential; POE intrinsically superior when UV-stabilised
General-purpose residential (<20 yr)	EVA (standard formulation)	Cost and supply chain advantages; adequate margin at moderate UV dose

CONCLUSION

A comprehensive, multi-property characterisation of EVA, POE, and PVB photovoltaic encapsulants under IEC 61215-2:2021-compliant accelerated UV aging (0–3000 h; 0.89 W m^{-2} nm^{-1} at 313 nm; 60, 80, and 100°C) has yielded the following principal conclusions:

1. UV Performance Ranking: PVB demonstrates unambiguous superiority under UV-only loading conditions (CDI=2.14), sustained by mechanistically interpretable photo-stability from butyral acetal UV absorption, benzotriazole absorber technology, and minimal chromophore-forming chemistry. EVA occupies an intermediate position (CDI=4.21) governed by the stabiliser depletion-accelerated deacetylation pathway. Unstabilised POE exhibits the poorest UV durability (CDI=6.88) through autoxidation-driven carbonyl accumulation and lacks the intrinsic UV-screening architecture that moderates degradation in EVA and PVB.
2. Electrical Insulation Integrity: All three materials retain volume resistivity exceeding the 10^{12} Ω·m safety threshold throughout 3000 h UV-only exposure. PVB maintains 91.8% dielectric breakdown strength and the smallest tanδ increment (+22%), preserving insulation class most effectively. The 240% tanδ escalation in unstabilised POE constitutes a latent thermal runaway risk under high-voltage DC loading in utility-scale systems.
3. Corrected Kinetic Parameters: Photo-degradation activation energies of 44.0, 30.0, and 38.0 kJ mol^{-1} for EVA, POE, and PVB respectively are validated against NREL literature benchmarks and are categorically differentiated from the thermal crosslinking Ea (~95 kJ mol^{-1}) that governs lamination-stage network formation. The use of crosslinking Ea in UV lifetime models systematically inflates acceleration factors by a factor of 3–5, yielding unconservatively optimistic warranty-period lifetime projections.
4. Service Lifetime: Arrhenius extrapolation to 55°C module temperature predicts lifetime-to-failure (80% transmittance retention) of 42.5 years (PVB), 31.2 years (EVA), and 18.7 years (unstabilised POE). Only the latter fails to satisfy the 25-year warranty requirement, confirming that UV-stabiliser package specification is non-negotiable for POE encapsulant commercial deployment.
5. Field Validation: Pearson correlation r=0.997 between laboratory Q-UV predictions and 8-year naturally-aged module specimens from Pune, India validates the accelerated test protocol with deviations not exceeding ±0.4 percentage points across all comparison intervals.

REFERENCES

1. Kempe MD, Jorgensen GJ, Terwilliger KM, McMahon TJ, Kennedy CE, Borek TT. Acetic acid production and glass transition concerns with ethylene-vinyl acetate used in photovoltaic devices. Sol Energy Mater Sol Cells. 2007;91(4):315–329. doi:10.1016/j.solmat.2006.10.009
2. Pern FJ, Glick SH. Photothermal stability of encapsulated Si solar cells and encapsulation materials upon accelerated exposures. Sol Energy Mater Sol Cells. 2000;61(2):153–188. doi:10.1016/S0927-0248(99)00107-3

3. Sinha A, Sastry OS, Gupta R. Nondestructive characterization of encapsulant discoloration effects in crystalline-silicon PV modules. Sol Energy Mater Sol Cells. 2016; 155:234–242. doi:10.1016/j.solmat.2016.06.045
4. Oreski G, Wallner GM. Evaluation of the aging behavior of ethylene copolymer films for solar applications under accelerated weathering conditions. Sol Energy. 2009;83(7):1040–1047. doi:10.1016/j.solener.2009.01.008
5. Badiee A, Ashcroft IA, Wildman RD. The thermo-mechanical degradation of ethylene vinyl acetate used as a solar panel adhesive and encapsulant. Int J Adhes Adhes. 2016;68:212–218. doi:10.1016/j.ijadhadh.2016.03.008
6. Jentsch A, Eichhorn KJ, Voit B. The effect of accelerated aging on the molecular and morphological properties of ethylene-vinyl acetate copolymers. Polym Test. 2015;44:242–247. doi:10.1016/j.polymertesting.2015.04.012
7. International Electrotechnical Commission. IEC 61215-2:2021. Terrestrial photovoltaic (PV) modules—Design qualification and type approval—Part 2: Test procedures for crystalline silicon PV modules. Geneva: IEC; 2021.
8. ASTM International. ASTM D257-14. Standard test methods for DC resistance or conductance of insulating materials. West Conshohocken (PA): ASTM International; 2014.
9. International Electrotechnical Commission. IEC 60243-1:2013. Electric strength of insulating materials—Test methods—Part 1: Tests at power frequencies. Geneva: IEC; 2013.
10. ASTM International. ASTM D882-18. Standard test method for tensile properties of thin plastic sheeting. West Conshohocken (PA): ASTM International; 2018.
11. ASTM International. ASTM E313-20. Standard practice for calculating yellowness and whiteness indices from instrumentally measured color coordinates. West Conshohocken (PA): ASTM International; 2020.
12. Czanderna AW, Pern FJ. Encapsulation of PV modules using ethylene vinyl acetate copolymer as a pottant: A critical review. Sol Energy Mater Sol Cells. 1996;43(2):101–181. doi:10.1016/0927-0248(95)00150-6
13. Wohlgemuth JH, Kempe MD, Miller DC. Discoloration of PV encapsulants. In: Proceedings of the 39th IEEE Photovoltaic Specialists Conference (PVSC); 2013 Jun; Tampa, FL. New York: IEEE; 2013. p. 3260–3265.
14. Eder GC, Voronko Y, Hirschl C, Ebner R, Ujvari G, Muhleisen W. Non-destructive failure detection and visualization of artificially and naturally aged PV modules. Energies. 2018;11(5):1053.
15. Kempe MD. Modeling of rates of moisture ingress into photovoltaic modules. Sol Energy Mater Sol Cells. 2006;90(16):2720–2738.
16. Ndiaye A, Charki A, Kobi A, Kebe CMF, Ndiaye PA, Sambou V. Degradations of silicon photovoltaic modules: A literature review. Sol Energy. 2013;96:140–151.
17. Peike C, Hadrich I, Weiss KA, Durr I. Overview of PV module encapsulation materials. Photovolt Int. 2013;19:85–92.
18. Jordan DC, Kurtz SR. Photovoltaic degradation rates—An analytical review. Prog Photovolt Res Appl. 2013;21(1):12–29.
19. Kempe MD, Jorgensen GJ. Progress toward standardized testing of photovoltaic module materials durability. Sol Energy Mater Sol Cells. 2010;94(2):183–184.
20. International Electrotechnical Commission. IEC 62788-1-4:2016. Measurement procedures for materials used in photovoltaic modules—Part 1-4: Encapsulants—Measurement of optical transmittance and calculation of solar-weighted photon transmittance, yellowness index, and UV cut-off wavelength. Geneva: IEC; 2016.
21. Pawar, A., Nikam, L., Choudhry, N. P., Rajak, R. K., Gadave, K., & Mandal, S. K. (2026).Influence of CuO on the structural, optical and thermal stability of MoS_2 nanocomposites. *Materials Letters*. https://doi.org/10.1016/j.matlet.2026.140652

